SAND2018-12119C

Full-Field Strain Shape Estimation From 3D SLDV

Bryan Witt, Dan Rohe and Tyler Schoenherr
Sandia National Laboratories*
P.O. Box 5800 - MS0557
Albuquerque, NM, 87185
blwitt@sandia.gov, dprohe@sandia.gov, tfschoe@sandia.gov

ABSTRACT

The ability to measure full-field strains is desirable for analytical model validation or characterization of test articles for which there is no model. Of further interest is the ability to determine if a given environmental test's boundary conditions are suitable to replicate the strain fields the test article undergoes in service. In this work, full-field strain shapes are estimated using a 3D scanning laser Doppler vibrometer and several post-processing methods. The processing methods are categorized in two groups: direct or transformation. Direct methods compute strain fields with only spatial filtering applied to the measurements. Transformation methods utilize SEREP shape expansion/smoothing of the measurements in conjunction with a finite element model. Both methods are used with mode shapes as well as operational deflection shapes. A comparison of each method is presented. It was found that performing a SEREP expansion of the mode shapes and post-processing to estimate strain fields was very effective, while directly measuring strains from ODS or modes was highly subject to noise and filtering effects.

Keywords: Laser, Vibrometer, Strain, Full-field, Expansion

1 INTRODUCTION

The capability to experimentally derive full-field strain response is of interest for several application areas such as model validation, fatigue life estimation, test object characterization, and determining the effectiveness of a test fixture to reproduce the damage potential seen in actual service. Full-field measurements are only now practically achievable thanks to advances in optical methods such as digital image correlation (DIC) and 3D scanning laser Doppler vibrometry (SLDV). DIC is a well-established method for full-field strain measurements but is not always the method of choice for a given test object. Cazzolato et al [1] demonstrated in 2008 that the state of 3D SLDV was such that strain measurements were feasible, but very sensitive to noise and issues such as quantization errors and laser head/specimen alignment. Weisbecker et al [2] further studied the sensitivities of using 3D LDV for strain measurements, including issues of laser head alignment, measurement mesh size, and the selection of spatial filter parameters (Savitzky-Golay differentiation filter). Reyes and Avitabile [3] among others have since applied 3D SLDV strain measurements on more complicated objects such as wind turbine blades, also demonstrating that results are highly subject to noise and related measurement issues.

Where previous works have focused on direct strain comparisons between 3D SLDV and finite element (FE) results or strain gage measurements, this work looks to develop a mode-based model of full-field strain shapes. This approach was taken for several reasons, the most poignant being the ability to determine which modes are the most damaging to an object and at

---

* Sandia National Laboratories is a multimission laboratory managed and operated by National Technology and Engineering Solutions of Sandia, LLC., a wholly owned subsidiary of Honeywell International, Inc., for the U.S. Department of Energy's National Nuclear Security Administration under contract DE-NA-0003525.

which physical location. With this information and an applied environment, the total strain response can be determined as a superposition of the modal strains. Further, this allows for the direct comparison, on a mode-by-mode basis, of an object's strain field in actual service versus in a test fixture. This provides a means to determine if a test fixture provides the correct boundary conditions/structural dynamic characteristics for an appropriate environmental test; often a test fixture does not provide the correct dynamics to generate the same damage potentials encountered in actual service.

Multiple methods for establishing full-field modal strains using 3D SLDV are evaluated for a moderately complicated test structure. The methods fall into two categories: direct or transformation. The direct methods employ spatial filtering prior to taking derivatives of measured shape displacements to arrive at strain shapes. The transformation methods use mode shapes or operational deflection shapes (ODS) as basis functions to expand and/or smooth the measured data prior to taking derivatives of measured shape data to arrive at strain shapes. The use of some type of basis functions to reduce noise in measured data was proposed in [1]. Expansion and smoothing are both done using the System Equivalent Reduction/Expansion Process (SEREP) [4]. Expansion of limited measured points to an augmented set of points requires the availability of a finite element model (FEM), whereas smoothing alone can be achieved with only measured shapes.

2 TEST STRUCTURE AND SETUP

The test article is a jointed aluminum assembly, taken from the "Box Assembly with Removable Component," or BARC test structure, that is currently used in many boundary condition assessment studies [5]. In this work, the "Removable Component," comprising two C-channel legs and a flat top member (see Fig. 1(b)), is taken as the object of interest. To simulate a typical environmental test setup, the "bench" is bolted to a fixture plate which is in turn affixed to a 7" vibration cube that would mount to a shaker table. The object was to identify full-field modal strain shapes of the bench when rigidly affixed to its test fixturing.

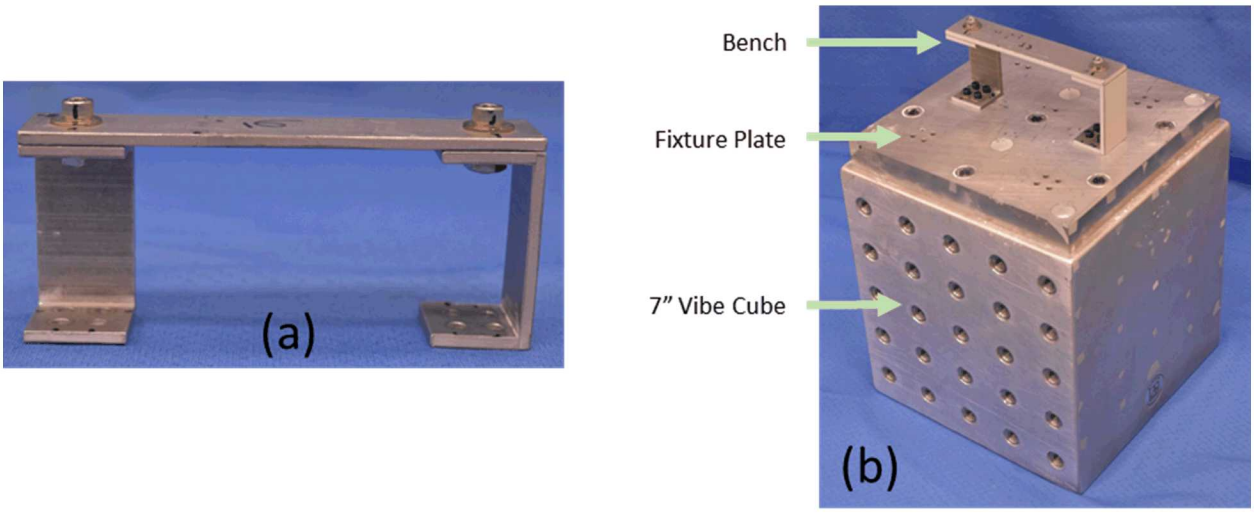

Fig. 1 Test article (a) and test configuration (b)

Measurements were taken with a Polytec PSV-500 Xtra (Infrared laser heads) 3D SLDV system. As shown in Fig. 2, the LDV heads are supported by a frame made from optical railing and the test object is supported on soft foam to approximate a free-free boundary condition for modal parameter estimations. Two electromagnetic shakers were placed at oblique angles on perpendicular sides of the vibration cube to provide excitation in multiple directions. Two front surface mirrors were placed at angles on either side of the test object to allow LDV measurements on three sides (front, left, right) without having to move the test article or laser heads between scans. The scan points are shown as blue markers in Fig. 3, which is a view from the LDV system's camera. Retroreflective tape was applied at all scan point locations to increase signal return to the LDV heads. A moderately dense 13x21 measurement grid was placed on the C-channel leg faces, while a single row of points was measured along the top beam and C-channel edges. Placement of the shakers and mirrors to have a view of three faces simultaneously drove the camera field of view to be wide relative to the areas of interest, meaning that the pixels per inch in the camera view were not optimized in any sense.

Two types of excitation methods were used: random and sine-dwell. Random excitation tests were used to obtain the displacement mode shapes and natural frequencies, ($\boldsymbol{E}$, $\boldsymbol{\omega}$). The random signal had a bandwidth of 10-6,400 Hz and Hann windowing was used with 50 averages. Sine-dwell tests were used to obtain ODS at the $\boldsymbol{\omega}$ frequencies identified from the random data, ($\boldsymbol{O}$, $\boldsymbol{f}$). The sine-dwells used 100 averages and produced ODS that were overall less noisy than those obtained

from the random testing. For both tests, the vibrometer was set for a measurement bandwidth of 1-6,400 Hz, a sample frequency of 16,000 and a 1 Hz resolution. Signal Enhancement set to Standard and Speckle Tracking enabled.

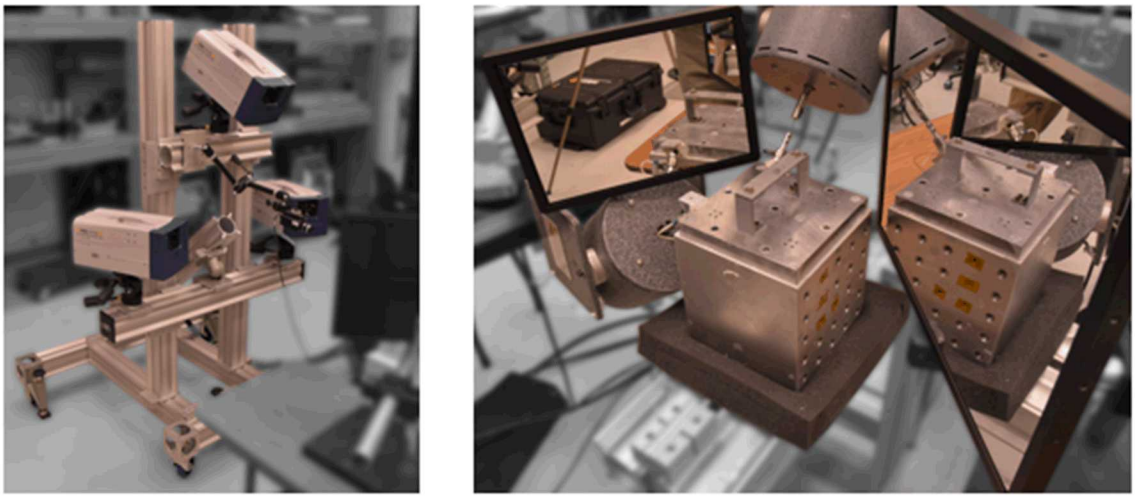

Fig. 2 Physical setup for modal testing

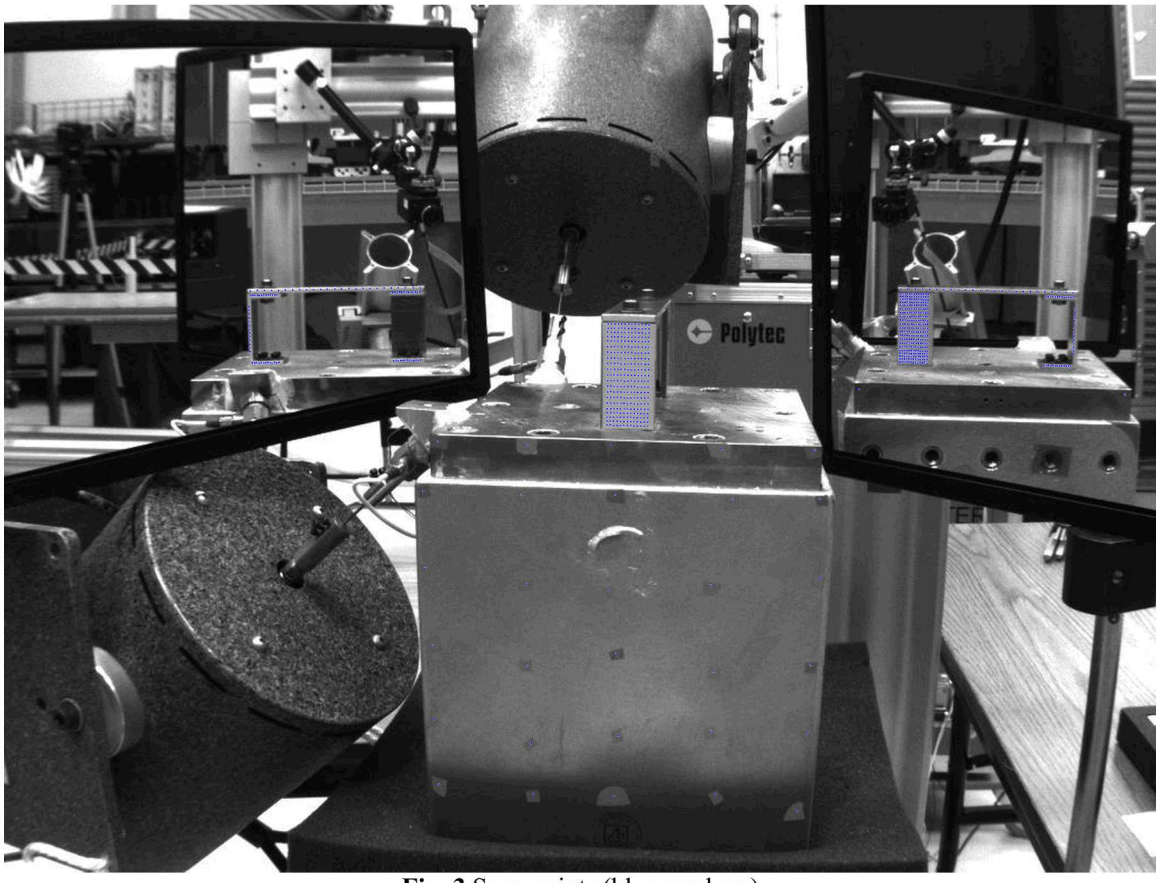

Fig. 3 Scan points (blue markers)

3 OVERVIEW OF METHODS AND TOOLS

An overview of the methods used in this work to derive full-field strain shapes is shown in Fig. 4. This flowchart will be discussed at length in the following sections. Within these methods there are three general tools (blue boxes in Fig. 4) that will be discussed in this section: Gaussian spatial filters, a strain post-processor, and SEREP.

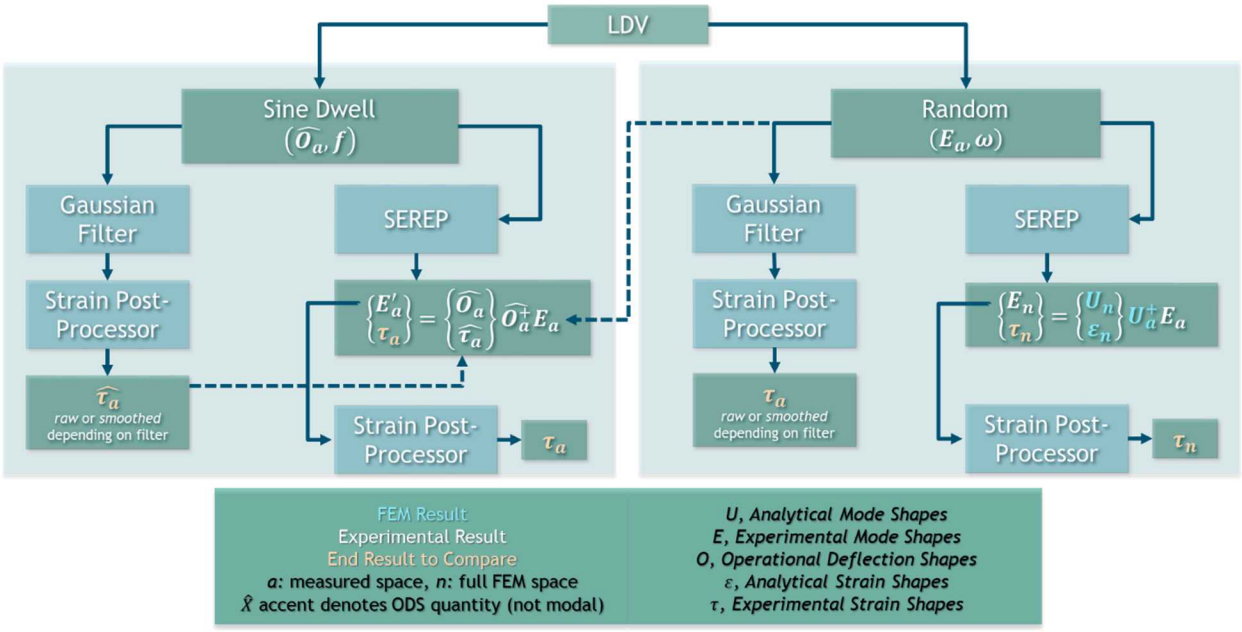

Fig. 4 Overview of full-field strain derivation methods studied

3.1 Gaussian Filter

The raw measured displacements from LDV systems can be noisy relative to accelerometer data, which is exacerbated when differentiating to obtain strain. Previous works, including [1-4], have emphasized the importance of applying spatial filtering to address the noise in measured displacements. In this work, the displacements are shape functions, either ODS or modal displacement shapes. In the direct methods used in this work, a 2D Gaussian spatial filter is applied as a low-pass smoothing function prior to calculating strains. The i^{th} filter weight for the j^{th} point is given by:

$$w_{ij} = \frac{1}{\sigma\sqrt{2\pi}} \left(\frac{\|\mathbf{r}_i - \mathbf{r}_j\|}{\sigma} \right)^2 \tag{1}$$

where the σ parameter is the size (e.g. 2.5 mm) and **r** are the coordinates of the measured points. The filtered displacement for the j^{th} point can then be calculated as:

$$\overline{d_j} = \frac{\sum_i w_{ij} d_i}{\sum_i w_{ij}} \tag{2}$$

An example 3D representation of filter weights on one of the bench's c-channel faces is shown in Fig. 5(a), along with a raw ODS (b) and the same ODS after the spatial filter was applied (c).

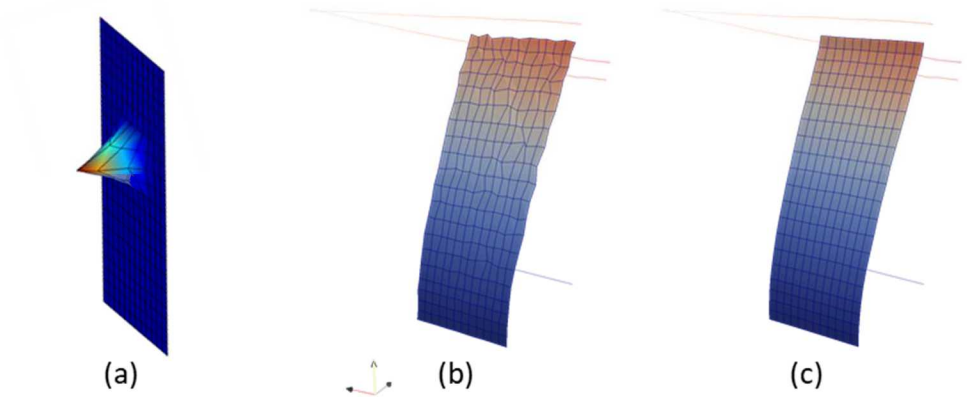

Fig. 5 Gaussian spatial filtering: (a) weighting coefficients, (b) raw shape, (c) filtered shape

3.2 Strain Post-Processor

In this work, the displacements are arbitrary shapes (mode shapes or ODS) rather than directly measured displacements. This posed an issue for using the Polytec strain post-processor, which operates on Band Data within their proprietary scan file format. Rather than creating a tool to write arbitrary shapes to a Band Data scan file, a standalone 2D strain post-processing script was written in MATLAB (note, 3D implementations will work equally well). Measured data from the SLDV system were exported in Universal File Format, which included the test geometry. The geometry node coordinates were in 3D (x,y,z) but were reduced to 2D surface coordinates (x,y) for each surface of interest. Node coordinates (x,y) and connectivity information were extracted from these files to create elements. Elemental deformations were either the experimental mode shapes ($\boldsymbol{E}$) estimated from the SLDV data using Synthesize Modes and Correlate (SMAC) [6] or ODS ($\widehat{\boldsymbol{O}}$) that were extracted directly from Polytec "Fastscan" data. With geometry and displacement data, strains were then calculated using a bilinear quadrilateral element formulation as detailed in [7] and summarized below. Strains were computed at the center of the element, $(\xi, \eta) = (0,0)$, and interpolated to a common set of points with the FEM so the measured results could be directly compared to analytical results. The elemental coordinate system is shown in Fig. 6 and the element shape functions are given in Eq. 3:

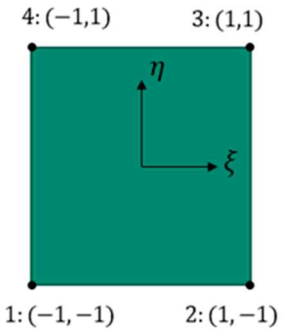

Fig. 6 Element nodes and coordinate system

$$
\begin{aligned}
N_1 &= \tfrac{1}{4}(1-\xi)(1-\eta) \\
N_2 &= \tfrac{1}{4}(1+\xi)(1-\eta) \\
N_3 &= \tfrac{1}{4}(1+\xi)(1+\eta) \\
N_4 &= \tfrac{1}{4}(1-\xi)(1+\eta)
\end{aligned}
\tag{3}
$$

The Jacobian matrix of (x,y) with respect to (ξ, η), denoted as $\boldsymbol{J}$, is used to establish the relationship between the derivatives of physical and elemental displacement:

$$
\begin{bmatrix} \frac{\partial N_i}{\partial x} \\ \frac{\partial N_i}{\partial y} \end{bmatrix} = \boldsymbol{J}^{-1} \begin{bmatrix} \frac{\partial N_i}{\partial \xi} \\ \frac{\partial N_i}{\partial \eta} \end{bmatrix}; \quad \boldsymbol{J} = \begin{bmatrix} \frac{\partial x}{\partial \xi} & \frac{\partial y}{\partial \xi} \\ \frac{\partial x}{\partial \eta} & \frac{\partial y}{\partial \eta} \end{bmatrix} \tag{4}
$$

where the differential entries of $\boldsymbol{J}$ are obtained through Eq. (5) below.

$$
\frac{\partial x}{\partial \xi} = \sum_i x_i \frac{\partial N_i}{\partial \xi}, \quad \frac{\partial y}{\partial \xi} = \sum_i y_i \frac{\partial N_i}{\partial \xi}, \quad \frac{\partial x}{\partial \eta} = \sum_i x_i \frac{\partial N_i}{\partial \eta}, \quad \frac{\partial y}{\partial \eta} = \sum_i y_i \frac{\partial N_i}{\partial \eta} \tag{5}
$$

Finally, strains are calculated using the strain-displacement matrix, $\boldsymbol{B}$, composed of the differentials calculated above and measured displacements, denoted here as (u,v) representing either ODS or mode shape coefficients.

$$
\boldsymbol{\tau} = \begin{bmatrix} \tau_{xx} \\ \tau_{yy} \\ 2\tau_{xy} \end{bmatrix} = \begin{bmatrix} \frac{\partial N_1}{\partial x} & 0 & \frac{\partial N_2}{\partial x} & 0 & \dots & \frac{\partial N_m}{\partial x} & 0 \\ 0 & \frac{\partial N_1}{\partial y} & 0 & \frac{\partial N_2}{\partial y} & \dots & 0 & \frac{\partial N_m}{\partial y} \\ \frac{\partial N_1}{\partial y} & \frac{\partial N_1}{\partial x} & \frac{\partial N_2}{\partial y} & \frac{\partial N_2}{\partial x} & \dots & \frac{\partial N_m}{\partial y} & \frac{\partial N_m}{\partial x} \end{bmatrix} \begin{Bmatrix} u_1 \\ v_1 \\ u_2 \\ v_2 \\ u_3 \\ v_3 \\ u_4 \\ v_4 \end{Bmatrix} = \mathbf{Bu} \tag{6}
$$

3.3 SEREP

Model reduction and expansion techniques are based on developing a transformation matrix, $\boldsymbol{T}$, that maps between a reduced space model (a-space) and a full space (n-space) model. Methods such as Guyan and Dynamic Condensation, for example, use system mass and stiffness matrices to form the transformation matrix. SEREP however uses the full space mode shapes as the basis for the transformation matrix which allows for exact preservation of the mode shapes and frequencies, as well as the ability to arbitrarily select which modes and degrees of freedom (DOF) to include in the reduction/expansion [4]. The analytical mode shapes of a FEM in full n-space are denoted by $\boldsymbol{U}_n$, whereas the same shapes at a reduced set of a DOF are denoted by $\boldsymbol{U}_a$. The SEREP transformation between full and reduced space mode shapes is then:

$$\boldsymbol{T} = \boldsymbol{U}_n \boldsymbol{U}_a^+ \tag{7}$$

where $^+$ indicates a generalized inverse. Experimental mode shapes, $\boldsymbol{E}$, measured at a DOF can be expanded to the full FEM n-space DOF by:

$$\boldsymbol{E}_n = \boldsymbol{T}\boldsymbol{E}_a = \boldsymbol{U}_n \boldsymbol{U}_a^+ \boldsymbol{E}_a \tag{8}$$

This method is of course not without limitations and caveats in usage. While the FEM used does not need to be exactly correlated to the test data, it is imperative that the FEM shapes span the space of the experimental shapes for an accurate expansion. For this reason, analytical rigid body mode shapes must be retained. Also, to prevent $\boldsymbol{E}_n$ from being rank deficient, the number of DOF kept needs to be greater than the number of preserved modes ($a > m$). It is also intuitive that including analytical mode shapes dominated by components which were not measured or captured experimentally will cause issues in the expansion process.

An example of an experimentally measured mode shape is shown in Fig. 7(a). Using the FEM to create $\boldsymbol{T}$, the same shape expanded to full-space is shown in (b). This method was applied to all ten experimentally identified mode shapes, as shown in Fig. 8.

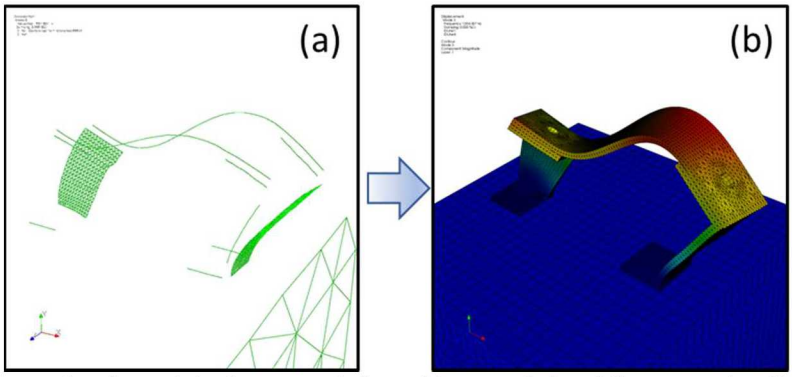

Fig. 7 Example of an original measured shape (a) expanded to full-space using SEREP (b)

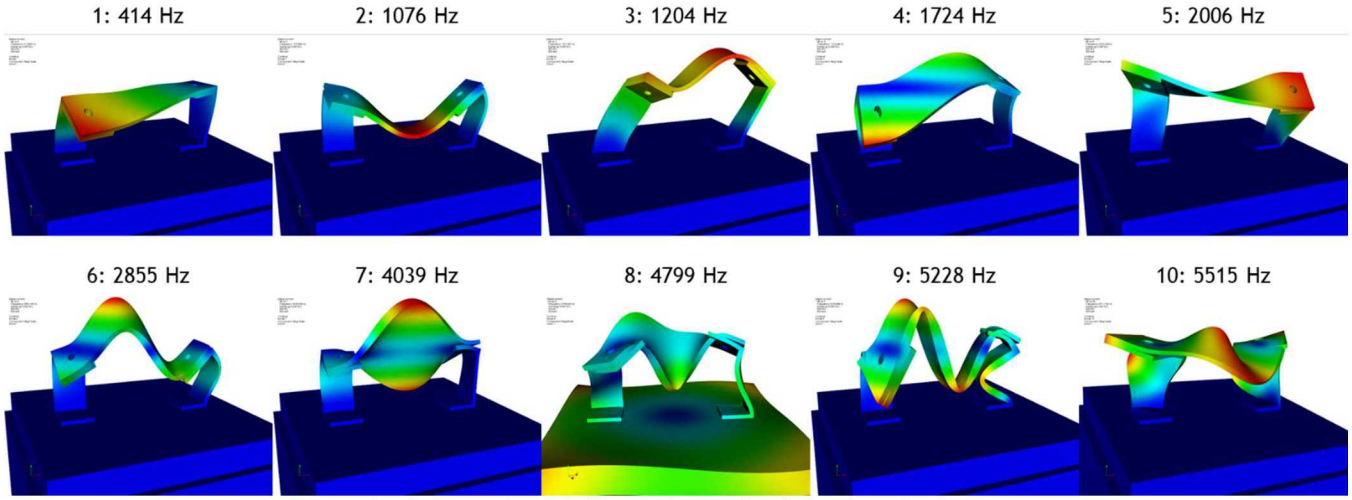

Fig. 8 Expansion of all experimentally derived mode shapes

The FEM used in this work was generally very well correlated to the test data, as shown by the modal assurance criterion (MAC) in Fig. 9. One of the experimental shapes did not have a match in the FEM (mode 8, large contribution from vibration cube), and experimental mode 9 was highly correlated to FEM shapes 14 and 15. Otherwise, the MAC values are quite good. Even so, the analytical FEM shapes still did not quite span the space of some of the experimental shapes, resulting in slightly imperfect expansions; two examples are shown in Fig. 10, where the experimental (mesh grid) and expanded shapes (solid) do not perfectly align.

MAC	Test Shapes									
FEM Shapes	1	2	3	4	5	6	7	8	9	10
1	0.02	0.18	0.08	0.00	0.02	0.08	0.02	0.03	0.05	0.05
2	0.16	0.01	0.03	0.02	0.18	0.02	0.00	0.04	0.00	0.09
3	0.07	0.09	0.27	0.00	0.02	0.10	0.01	0.00	0.03	0.03
4	0.48	0.02	0.02	0.34	0.01	0.00	0.09	0.10	0.03	0.03
5	0.00	0.18	0.58	0.01	0.01	0.20	0.00	0.01	0.13	0.03
6	0.22	0.01	0.00	0.03	0.38	0.00	0.00	0.14	0.00	0.28
7	0.99	0.02	0.00	0.14	0.01	0.00	0.05	0.00	0.00	0.04
8	0.03	0.95	0.02	0.03	0.00	0.16	0.02	0.00	0.07	0.00
9	0.00	0.17	0.95	0.04	0.01	0.10	0.00	0.02	0.09	0.01
10	0.10	0.03	0.00	0.95	0.00	0.02	0.02	0.01	0.04	0.04
11	0.01	0.01	0.01	0.07	0.93	0.01	0.00	0.03	0.01	0.11
12	0.00	0.19	0.12	0.02	0.00	0.99	0.01	0.01	0.20	0.00
13	0.05	0.03	0.00	0.01	0.01	0.00	0.98	0.01	0.00	0.00
14	0.00	0.12	0.09	0.08	0.01	0.21	0.00	0.11	0.97	0.00
15	0.01	0.12	0.08	0.07	0.00	0.22	0.00	0.02	0.93	0.02
16	0.05	0.00	0.01	0.04	0.17	0.00	0.01	0.08	0.01	0.96
17	0.04	0.15	0.04	0.04	0.00	0.22	0.06	0.01	0.20	0.00
18	0.06	0.02	0.04	0.15	0.00	0.07	0.03	0.07	0.24	0.04

Rigid Body Modes

Fig. 9 MAC between FEM and experimental mode shapes

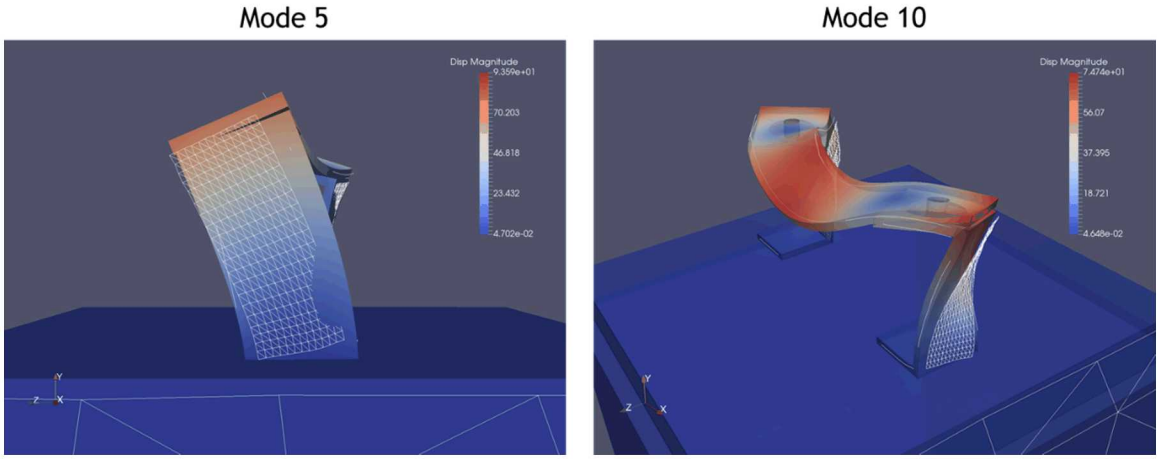

Fig. 10 Examples of imperfect shape expansions

Modal displacement vectors are used as the basis for the transformation in Eq. (8). However, the data can be expanded using other modal quantities as well. For example, if modal strain shapes from the FEM ($\boldsymbol{\epsilon}_n$) are available, they can be used in the expansion to arrive at full *n*-space strain shapes directly as:

$$\boldsymbol{\tau}_n = \boldsymbol{\varepsilon}_n \boldsymbol{U}_a^+ \boldsymbol{E}_a \tag{9}$$

SEREP can also be used as a least squares error minimization using shape vectors as the basis, removing variance from measured data. We can exploit this as a method to smooth noisy measured mode shapes ($\boldsymbol{E}_a$) using ODS (which potentially have a higher signal-to-noise ratio) in addition to using Gaussian spatial filters:

$$\boldsymbol{E}'_a = \widehat{\boldsymbol{O}_a} \widehat{\boldsymbol{O}_a}^+ \boldsymbol{E}_a \tag{10}$$

Similar to Eq. (9), we can alternatively choose to use ODS derived strain shapes ($\widehat{\boldsymbol{\tau}_a}$, discussed in the next section, can be extracted from $\widehat{\boldsymbol{O}_a}$ using Polytec's strain post-processor) as part of the basis for the smoothing, and directly arrive at smoothed modal strain shapes in the measured *a*-space:

$$\boldsymbol{\tau}_a = \widehat{\boldsymbol{\tau}_a} \widehat{\boldsymbol{O}_a}^+ \boldsymbol{E}_a \tag{11}$$

4 LDV DIRECT METHODS

As mentioned in the previous section, several methods for generating full-field modal strain shapes were utilized. All methods can be grouped into two categories: direct or transformation methods. This section focuses on the direct methods, which can be generated either on an ODS or modal quantity basis. Fig. 11 shows the two direct methods; the "Direct ODS Method" is the workflow on the left and the "Direct Modal Method" is the workflow on the right.

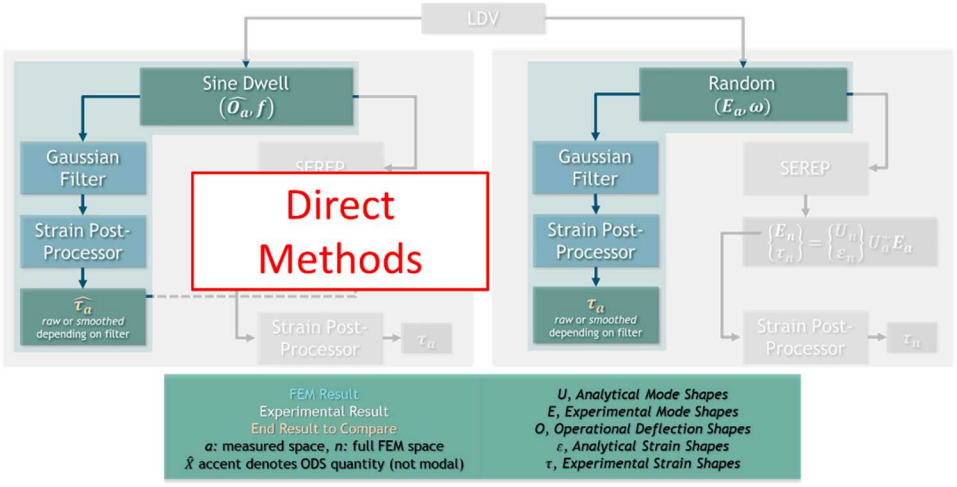

Fig. 11 Direct methods for strain shape estimation

In some cases, it is expected that ODS extracted from sine dwell data near natural resonance frequencies $(\widehat{\boldsymbol{O}_a}, \boldsymbol{f})$ at *a*-space measurement locations would be less noisy than traditionally fit mode shapes from LDV data $(\boldsymbol{E}_a)$. For example, if a sine-dwell test had a better signal-to-noise ratio than a random vibration test from which modes would be extracted, the Direct ODS Method could be used. The measured $\widehat{\boldsymbol{O}_a}$ should then be smoothed with a Gaussian filter. Note that a Gaussian filter of size σ less than approximately one third of the scan point spacing effectively provides no smoothing and leaves shapes in an unfiltered or raw state. Once any desired filtering is applied, the shapes can be run through the strain post-processor to arrive at an ODS-quantity estimation of the strain shapes in *a*-space, $\widehat{\boldsymbol{\tau}_a}$. For structures where the ODS well approximate the mode shapes (i.e. resonances well separated), $\widehat{\boldsymbol{\tau}_a}$ will, to the same degree, approximate the $\boldsymbol{\tau}_a$ modal strain shapes we are seeking, although they will be scaled differently. This method most closely aligns with the Polytec Strain Post-Processor that is integrated into the LDV software, which operates on Band Data within a scan file.

For applications where a modal test can be conducted and relatively clean mode shapes and natural frequencies $(\boldsymbol{E}_a, \boldsymbol{\omega})$ extracted, the Direct Modal Method can be utilized. The same process of smoothing shapes with a Gaussian spatial filter and post-processing the results for strain are used. In this case, the resulting $\boldsymbol{\tau}_a$ strain shapes are actual modal quantities.

Both Direct methods have the benefits of not requiring a FEM of the test object nor needing an expansion process for sufficiently dense measurement grids. However, both are subject to any noise in the measurements and are also highly dependent on the spatial filter parameters used. To demonstrate these effects, Gaussian filters with σ = 0.5–3.5 mm were evaluated. The scan grid on the c-channel faces of interest had a horizontal and vertical spacing of approximately 1.6 x 2.6 mm, respectively. This means that filter sizes of approximately 0.5 mm or less are providing almost no smoothing. Surface strains $(\boldsymbol{\tau_{xx}}, \boldsymbol{\tau_{yy}}, \boldsymbol{\tau_{xy}})$ in *a*-space were calculated for the two c-channel faces (X-surface and Z-surface, see Fig. 12), although only $\boldsymbol{\tau_{yy}}$ results on the X-face are shown here for brevity. Fig. 13 and Fig. 14 show the $\boldsymbol{\tau_{yy}}$ results of the Direct ODS Method and Direct Modal Methods, respectively, for multiple filter sizes. Black indicates noise values that are out of range.

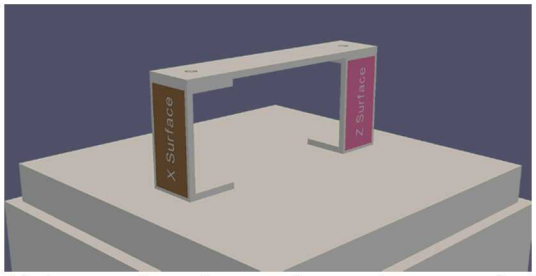

Fig. 12 Area patches where surface strains were calculated

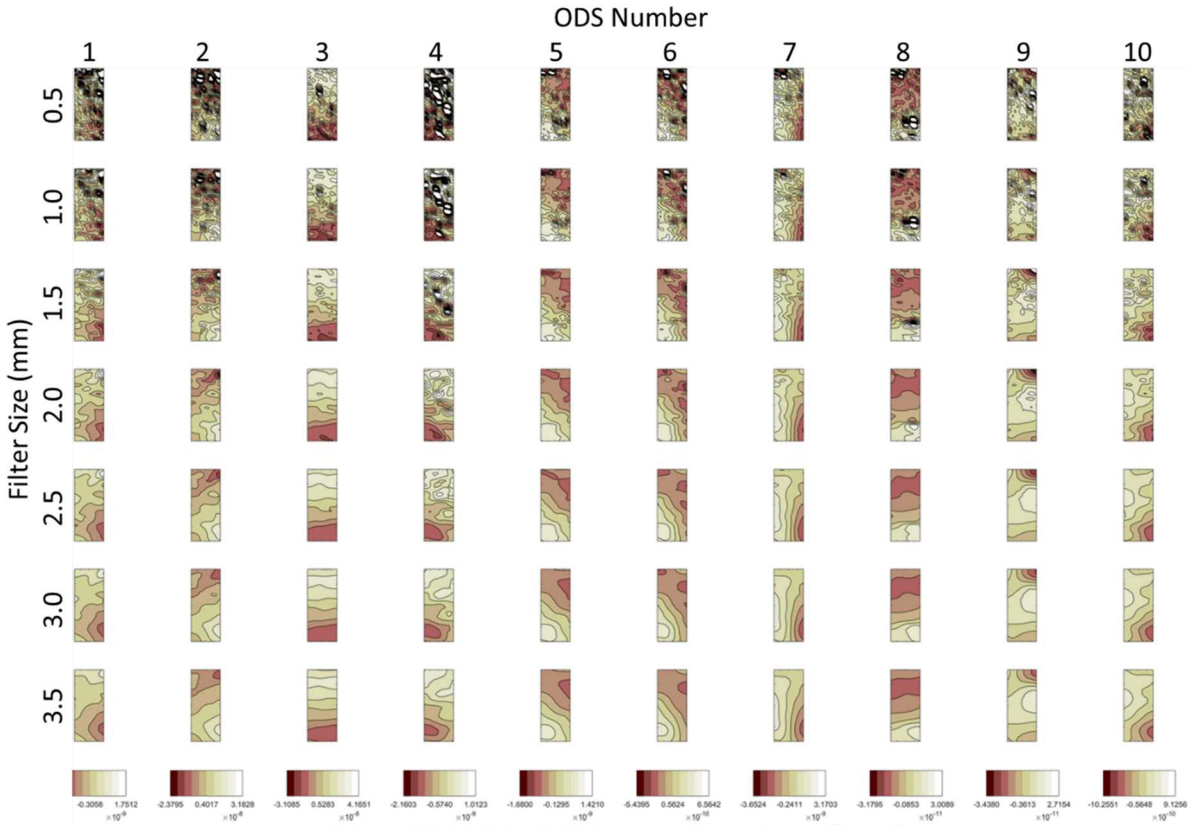

Fig. 13 Direct ODS Method: X-Face $\boldsymbol{\tau_{yy}}$ for multiple filter sizes

Fig. 14 Direct Modal Method: X-Face $\boldsymbol{\tau_{yy}}$ for multiple filter sizes

Both figures show that filter sizes greater than the nominal spacing of measurement points is necessary to remove spurious noise in the shapes, which is approximately 2.0 mm here. However, it is noted that the Direct ODS Method results for the 1.5 mm filter are noticeably noisier than their Modal counterparts, indicating the ODS for this test structure were not cleaner than the mode shapes, as had been postulated. The test article exhibited nonlinear behavior which is believed to be the reason for this observation. Filter effects near the edges are clearly observed in several shapes, for example ODS 5 and Mode 4; as filter weight increases, the maximum strains at the edges are artificially reduced due to the distribution of the weighting coefficients of the filter. There is a tradeoff between noise reduction and maximum strain accuracy, particularly near edges. Fig. 13 and Fig. 14 also illustrate the differences between ODS and modal strain shapes, even for a structure whose modes are well spaced and the ODS are very similar to the mode shapes, as illustrated by the MAC between the two in Fig. 15.

MAC		Mode Shapes									
		1	2	3	4	5	6	7	8	9	10
ODS	2	0.99	0.03	0.00	0.15	0.01	0.00	0.06	0.00	0.00	0.05
	3	0.02	0.99	0.11	0.02	0.01	0.17	0.03	0.00	0.08	0.00
	4	0.00	0.09	0.95	0.01	0.03	0.09	0.00	0.00	0.04	0.01
	5	0.11	0.02	0.01	0.99	0.02	0.01	0.02	0.02	0.06	0.02
	7	0.00	0.00	0.00	0.01	0.95	0.00	0.00	0.04	0.01	0.17
	8	0.01	0.15	0.10	0.03	0.01	0.88	0.00	0.00	0.13	0.01
	9	0.05	0.04	0.00	0.01	0.00	0.00	0.99	0.02	0.00	0.00
	10	0.00	0.01	0.02	0.02	0.05	0.01	0.01	1.00	0.14	0.11
	11	0.00	0.10	0.06	0.07	0.01	0.19	0.00	0.08	0.98	0.01
	12	0.05	0.01	0.02	0.02	0.17	0.00	0.00	0.12	0.00	0.98

Fig. 15 MAC between ODS and mode shapes

5 LDV TRANSFORMATION METHODS

The second category of methods utilize transformations to derive full-field modal strain shapes, as shown in Fig. 16.

The workflow on the right side of the figure will be referred to as the "Transformation Modal Method". In this method, the displacement mode shapes extracted from a measurement points ($\boldsymbol{E}_a$) are expanded to the full FEM n-space using SEREP, as shown in Eq. (8). These $\boldsymbol{E}_n$ shapes are then post-processed to obtain full n-space modal strain shapes $\boldsymbol{\tau}_n$. Alternatively, if the FEM includes analytical strain shapes ($\boldsymbol{\varepsilon}_n$), the expansion in Eq. (9) can be used to directly arrive at the same $\boldsymbol{\tau}_n$ without the need to use a standalone strain post-processor. Provided that strains are calculated the same in the FEM as the standalone strain post-processor, these two variations will be identical and only circumstance would dictate which should be used. In this work, $\boldsymbol{\varepsilon}_n$ were available from the FEM, so Eq. (9) is used for the Transformation Modal Method results herein, but the alternative path was also computed to verify they produce equivalent results.

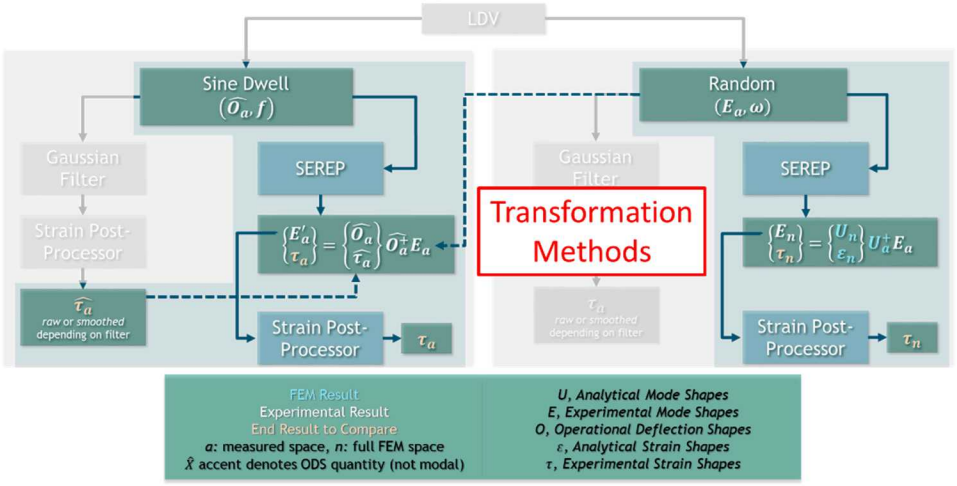

Fig. 16 Transformation methods for strain shape estimation

On the left side of Fig. 16 is the so-called "Transformation ODS Method", although it is noted that both ODS $\widehat{\boldsymbol{O}_a}$ and mode shapes $\boldsymbol{E}_a$ are required. It should be noted that while this method required both shape sets, it does not need a FEM of the test object. The first variation would be to use the ODS to smooth the measured mode shapes per Eq. (10) and then post-process to obtain modal strain shapes $\boldsymbol{\tau}_a$. It was observed in our application that the smoothed $\boldsymbol{E}'_a$ was still too noisy to calculate

strains and required the additional application of a Gaussian filter prior to being post-processed for strains. Note that the results are in the measured *a*-space, as the SEREP implementation here is for smoothing only and does not involve an expansion to *n*-space. The second variation of this method is to first calculate an ODS based set of strain shapes $\widehat{\boldsymbol{\tau}_a}$ using either the Direct ODS Method or the Polytec Strain Post-Processor, which then feeds into Eq. (11) to directly arrive at *modal* strain shapes in *a*-space, $\boldsymbol{\tau}_a$. These two variations are mathematically identical, as can be shown by combining Eq. (6) and Eqs. (10,11):

$$\begin{aligned} \text{variation 1: } \boldsymbol{\tau}_a &= \boldsymbol{B}\boldsymbol{E}'_a = \boldsymbol{B}\boldsymbol{W}\widehat{\boldsymbol{O}_a}\widehat{\boldsymbol{O}_a}^{+}\boldsymbol{E}_a \\ \text{variation 2: } \boldsymbol{\tau}_a &= \widehat{\boldsymbol{\tau}_a}\widehat{\boldsymbol{O}_a}^{+}\boldsymbol{E}_a = \boldsymbol{B}\boldsymbol{W}\widehat{\boldsymbol{O}_a}\widehat{\boldsymbol{O}_a}^{+}\boldsymbol{E}_a \end{aligned} \tag{12}$$

where $\boldsymbol{W}$ is the applied Gaussian filter weights matrix. Although these variations produce identical results, we choose to leave them as different workflows to point out the two usage cases: (1) a modal test is performed, $\boldsymbol{E}_a, \widehat{\boldsymbol{O}_a}$ are both obtained and a standalone strain post-processing is performed to generate modal strain shapes, versus (2) a modal test is performed in conjunction with Fastscan testing via the Polytec LDV system and the results are combined to generate modal strain shapes.

The FEM was delivered with 300 modes and 127,155 DOF. Ten modes were experimentally extracted from the modal test in which 2202 DOF were measured (*a*-space set) with the 3D SLDV system. Using SEREP, the FEM was reduced to 20 DOF and the first 18 analytical shapes were retained, which includes the rigid body modes and excludes modes dominated by the vibration cube, since these were not well measured in the modal test. These were used in the Transformation Modal Method calculations.

Twelve ODS were extracted from the sine dwell data (first 10 shown in figures below). A total of 2202 DOF were measured with the 3D SLDV system, corresponding to the same set as the modal test. All DOF (*a*-space set) and all extracted ODS were retained in the SEREP smoothing step of the Transformation ODS Method. Example results from the Transformation ODS and Transformation Modal Methods are shown in Fig. 17 and Fig. 18, respectively, for the $\boldsymbol{\tau}_{yy}$ component of strain on the X-Face of the c-channel support (see Fig. 12). As mentioned above, the smoothed $\boldsymbol{E}'_a$ shapes in the Transformation ODS Method were still too noisy to use directly for strain calculations, so Gaussian filters were applied, ranging in size from 0.5 to 3.5 mm as can be seen in Fig. 17.

Fig. 17 Transformation ODS Method: X-Face $\boldsymbol{\tau}_{yy}$ (both variations identical)

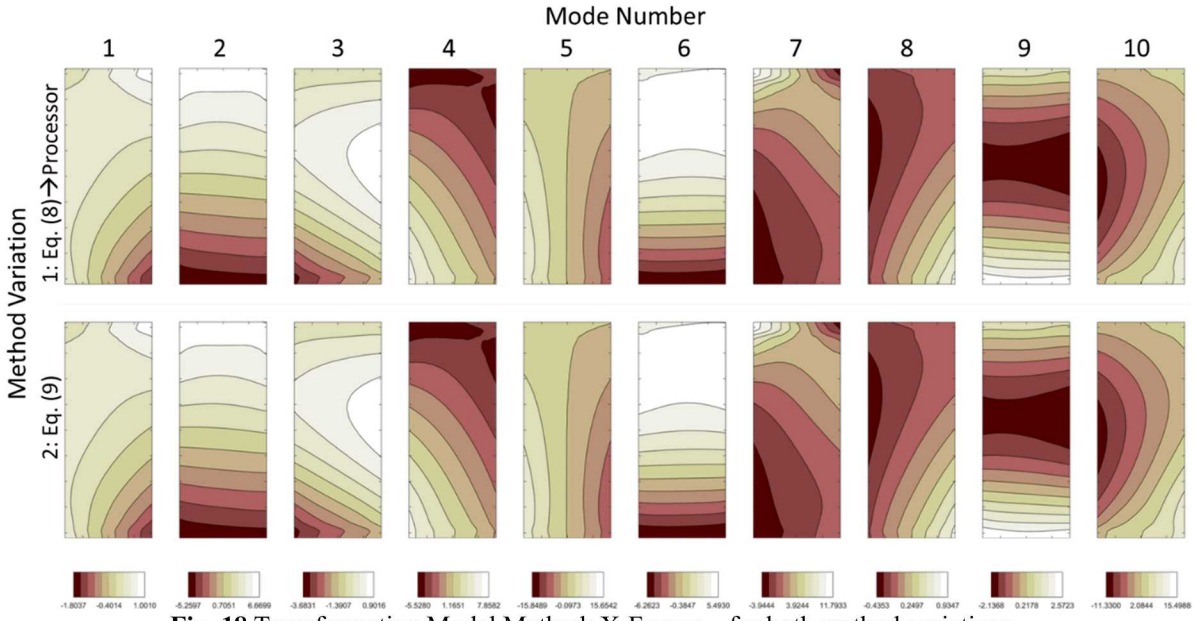

Fig. 18 Transformation Modal Method: X-Face $\boldsymbol{\tau_{yy}}$ for both method variations

The results shown in Fig18 are practically identical to each other because the standalone strain post-processor and the FEM calculated strains in the same manner. Overall, these results are very clean, are obtained in full *n*-space, and do not exhibit filter edge effects that the methods which utilize the spatial filters suffer from. Further, the Transformation Modal Method measurement *a*-space does not actually need to approach full-field; only enough measurement DOF to adequately describe the shapes for the expansion process are required to then obtain full-field modal strain shapes.

6 COMPARISON OF METHODS

Comparing all four methods is not trivial due to the differences in scaling between ODS strain shapes and modal strain shapes. The MAC between the ODS and mode shapes was used to match ODS to shapes for comparison of the first six mode shapes. The scaling is different between ODS and modal shapes as well. For comparison of the methods which utilize a Gaussian filter, results from the 3.0 mm filter size were selected based on the overall tradeoff between edge effects and noise reduction. Fig. 19 shows this final comparison between each of the methods and the FEM for the $\boldsymbol{\tau_{yy}}$ component of strain on the c-channel X-face. The remaining components of strain were calculated for this and the Z-face as well but are omitted for brevity as the results are typical in each case.

The traditional Direct ODS method produces very usable results, which are comparable to the Transformation ODS in terms of noise. However, the results have the disadvantage of not being actual modal quantities. Although ODS data may be obtained with the 3D SLDV much more rapidly than a modal test with the same number of measured DOF, there is an advantage to extracting the modal parameters to use in the strain estimation, as evidenced by the difference between Direct ODS and Direct Modal methods. While Direct Modal is still in *a*-space, it is obviously a smoothed modal quantity which was a desired attribute of this work, and the results are good considering no FEM was required.

The Transformation ODS Method admittedly does not appear to be much of an improvement over the Direct ODS results, but does render modal quantity results. The comparison to Direct Modal is comparable; both are in *a*-space, have similar sensitivity to measurement noise, and suffer from filter edge effects. Given the amount of work that the Transformation ODS Method takes compared to the Direct Modal method, the latter would likely be an easier choice between the two. However, if Polytec Fastscan data and Strain Post-Processor are to be used, the Transformation ODS Method can be used to obtain modal strain shapes from that data.

Finally, the Transformation Modal Method is found to perform very well. The method is very robust against measurement noise, does not suffer from filter edge effects and provides results in full *n*-space. The obvious downside is the requirement to have a FEM of your test object. The FEM does not have to be perfectly correlated to test data, however the analytical shapes must span the space of the experimental shapes. The comparison of the experimental full-field modal strain shapes from the Transformation Modal Method to the FEM is expectedly very good, since they are a superposition of FEM shapes. The results may be a better indication of the actual strain fields than the FEM as they are experimentally derived and the model is

not fully correlated. While surface strains were of interest in this work due to use of the 3D SLDV measurements, we note that this method can provide experimentally derived full-field *n*-space *volume* strains as well by substituting their analytical FEM counterparts into Eq. (9) in place of $\boldsymbol{\varepsilon}_n$ surface strains.

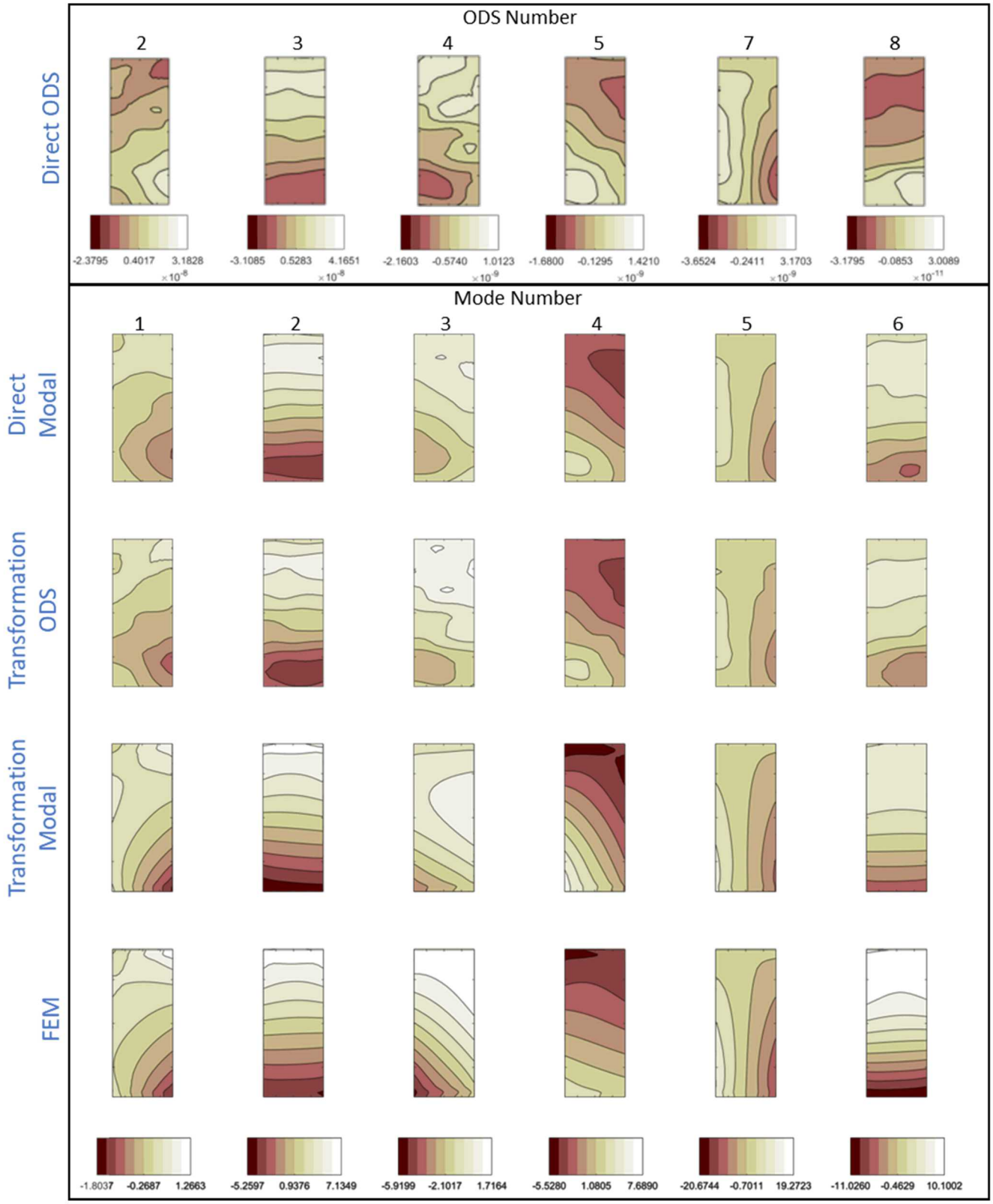

Fig. 19 Comparison of methods for X-face $\boldsymbol{\tau}_{yy}$

7 CONCLUSIONS

Several methods for determining full-field modal strain shapes from 3D SLDV data were evaluated. The Direct Modal method was found to work reasonably well, does not require a FEM, and provides improvements over the Direct ODS Method, which is considered as the current standard ODS strain shape measurement method. The use of direct measurements (ODS or modal) without some manner of filtering to smooth the displacements is not recommended due to the sensitivity to measurement noise in the strain estimation process. The Transformation ODS Method provides a means to convert ODS strain shapes to modal quantities, also without use of a FEM. However, if starting from nothing, the Direct Modal Method provided similar, if not better, results with less processing effort but potentially longer test times. Further, the SEREP smoothing using (noisy) ODS may not provide enough smoothing by itself, driving the need to use a spatial filter in addition. The test article used in this work was observed to exhibit nonlinear behavior, which is believed to have caused a reduction in the ODS methods' effectiveness. Finally, the Transformation Modal Method was shown to work very well; it is robust against measurement noise, avoids spatial filter edge effects, results are obtained in full *n*-space, and either surface or volume strains can be estimated. The primary drawback is that a FEM is required.

REFERENCES

[1] B. Cazzolato, S. Wildy, J. Codrington, et al, "Scanning laser vibrometer for non-contact three-dimensional displacement and strain measurements," *Proceedings of ACOUSTICS,* 24-26 November 2008, Geelong Australia.

[2] H. Weisbecker, B. Cazzolato, S. Wildy, et al, "Surface Strain Measurements Using a 3D Scanning Laser Vibrometer," *Experimental Mechanics*, Volume 52 Issue 7, pp. 805-815, September 2012.

[3] J. Reyes, P. Avitabile, "Use of 3D Scanning Laser Vibrometer for Full Field Strain Measurements", In: De Clerck J. (eds) *Experimental Techniques, Rotating Machinery, and Acoustics, Volume 8. Conference Proceedings of the Society for Experimental Mechanics Series*. Springer, 2015.

[4] J. O'Callahan, P. Avitabile, R. Riemer, "System Equivalent Reduction Expansion Process (SEREP)," *Proceedings of the 7th International Modal Analysis Conference*, 1989.

[5] D. Rohe, T. Schoenherr, T. Skousen, et al, "Testing Summary for the Box and Removable Component Structure," *Proceedings of the 37th International Modal Analysis Conference,* Orlando, Florida, January 2019.

[6] D. Hensley, R. Mayes, "Extending SMAC to Multiple References," *Proceedings of the 24th International Modal Analysis Conference,* pp. 220-230, February 2006.

[7] C. Felippa, *Introduction to Finite Element Methods* (2004), Chapter 17, Department of Aerospace Engineering Sciences, University of Colorado at Boulder, accessed online 2018: https://www.colorado.edu/engineering/CAS/courses.d/IFEM.d/